Culebras, M.; Sanchis Sánchez, MJ.; Beaucamp, A.; Carsí Rosique, M.; Kandola, BK.; Horrocks, AR.; Panzetti, G.... (2018). Understanding the thermal and dielectric response of organosolv and
modified kraft lignin as a carbon fibre precursor. Green Chemistry. 20(19):4461-4472. https://doi.org/10.1039/c8gc01577e

Understanding the thermal and dielectric response of organosolv and modified kraft lignin

Mario Culebras[a], Maria J. Sanchis[b], Anne Beaucamp[a,c] , Marta Carsí [b,d], Baljinder K. Kandola[e], A. Richard Horrocks[e], Gianmarco Panzetti[e], Colin Birkinshaw[f] and Maurice N Collins[a,c]*

[a]*Stokes Laboratories, Bernal Institute, University of Limerick, Ireland.*

[b]*Instituto Tecnológico de la Energía, Departamento de Termodinámica Aplicada, Universitat Politècnica de València, Camí de Vera s/n, 46022, Valencia, Spain*

[c]*School of Engineering, University of Limerick, Ireland.*

[d]*Instituto de Automática e Informática Industrial, Universitat Politècnica de Valencia, 46022 Valencia, Spain*

[e]*University of Bolton, Bolton, United Kingdom.*

[f] *Emeritus, Dept. Materials Science and Engineering, University of Limerick, Ireland*

***corresponding author**

Abstract

Understanding the thermal behaviour of lignin is crucial in order to realise its valorisation as an engineering polymer. Two hardwood lignins, organosolv (OSL) and chemically modified kraft lignin (ML) have been chosen to represent important classes of renewable and abundant raw material. The relationship between ionic mobility and viscosity in OSL and ML have been studied. The rheological results have been interpreted in terms of the competitive processes of thermal plasticisation and stiffening through crosslinking. Results show that with OSL crosslinking proceeds relatively rapidly, and this is consistent with its more reactive structure. Higher molecular weight (Mw) influenced the melt stability as cross-linking kinetics were reduced and this was attributed to the reduction of chain ends available for cross-linking reactions. Scanning calorimetry has shown that both materials are glassy and pass through the glass transition between 100 °C and 115 °C, with the higher molecular weight modified material having the slightly higher Tg. Both lignins show pronounced maxima in the Gramm-Schmidt plots for methane or methanol around 400°C. However, a significant difference between the materials is observed with the detection of a strong carbonyl peak in the evolution products of the ML, this is attributed to scission of the hydroxypropyl substituent present in the ML structure. The differences in the degradation processes are further reflected in the dielectric properties of the partially degraded materials where loss maxima occur at different temperatures, and show different degrees of frequency dependence. An important observation is the difference in conductivity, where higher values for OSL are attributed to cross-linking between adjacent benzene rings, whereas with the ML lower conductivity is associated with intrinsically less conductive intermolecular linkages. These results demonstrate that the thermal

decomposition of the two lignins, follow significantly different paths at the molecular level. With the more reactive OSL it appears to be the case that there is a greater tendency to form direct ring to ring crosslinks and this is very significant for the properties of the intended end product.

Keywords: Lignin; crosslinking; dielectric relaxation spectroscopy; rheology;carbon fibre

1. Introduction

The depletion of petroleum resources and their environmental impact has driven an increased interest in biobased materials [1, 2]. An abundant and renewable alternative is found in lignocellulosic biomass, hard and soft wood, straw corncob and other products from agriculture and forestry. Lignin along with cellulose is one of the most prevalent components of lignocellulosic biomass. Lignin is amorphous and the only aromatic biopolymer present in the cell wall of pith, roots, fruit, buds and bark. Currently, it is a non-valorised waste of the paper industry, and its degradation generates furans and dioxins which consume dioxygen [3-5]. The synthesis of lignin is carried out by the enzyme-initiated dehydrogenative random polymerisation of coniferyl alcohol, sinapyl alcohol and p-coumaryl alcohol [6, 7]. The polymerisation of these molecules generates a cross-linked and highly heterogeneous aromatic polymer whose chemical and physical properties are determined by syringyl (S), guaicyl (G), and *p*-hydroxyphenyl content, molecular weight, degree of branching, and purity [8]. It is known that its extraction method, for e.g. kraft/organosolv, influences these parameters [9]. Kraft lignin is obtained from the paper and pulp industry, the process involves the mixing of wood raw materials and liquor with sodium hydroxide and sodium sulphide at 150–180 ºC [6]. Organosolv lignin (OSL) is

produced through extraction from wood chips utilising organic solvents such as alcohols, ketones, and glycols under mildly acidic conditions [6, 10]. Soda lignin is obtained from a soda pulping process [10].

Lignin degradation can generate high value-added products such as: acetic acid, methanol, charcoal or other phenolic compounds [11]. Lignin is known to be an excellent additive for improving flame retardancy in polymeric materials, usually as a char-former present with phosphorus-based, Lewis acidic species such as ammonium and melamine phosphates or phytic acid [12-14] ; it can also provide antioxidant protection [15].

Carbon fibres are currently being deployed in structural applications due to their excellent physical properties such as: high stiffness and tensile strength, low thermal expansion and density, heat tolerance and reagent resistance [16]. The vast majority of carbon fibres are produced using wet and solution spun polyacrylonitrile (PAN), a costly production process with a large environmental footprint. Other researchers have studied lignin as a precursor fibre for carbon fibre, however, the mechanical properties obtained for carbon fibres based on lignin were shown to be brittle [17]. However, it has been claimed that improvements can be obtained through the optimisation of chemical reactions during the stabilization and carbonization processes [18] and the optimisation of thermal behaviour during each processing step [19].

For these reasons this work is focused on the study of the thermal behaviour of two different hardwood lignins, organosolv (OSL) and chemically modified kraft lignin (ML) (In general softwood lignin do not display thermoplastic and sometimes chemical modifications are required to increase the fusibility of lignin[20]). The samples were characterized by rheology, broadband dielectric relaxation spectroscopy (DRS), Fourier

transform infrared (FTIR), differential scanning calorimetry (DSC) and thermogravimetric analysis coupled with FTIR (TGA-FTIR) providing a comprehensive explanation of the thermal transitions occurring during the processing of lignin carbon fibre precursors. The potential of dielectric impedance spectroscopy in monitoring the progress of structure/property relationships in lignin is demonstrated through correlations between dielectric and chemo-rheological phenomena.

2. Experimental

2.1 Materials

Organosolv Lignin (Mw=3952 g/mol and PDI=4.69) (OSL) and hydroxypropyl modified lignin (Mw=11357 g/mol and PDI=4.58) (ML) were supplied by Tecnaro (Ilsfeld, Germany). The structure of lignins used in this study is shown in **Figure 1**.

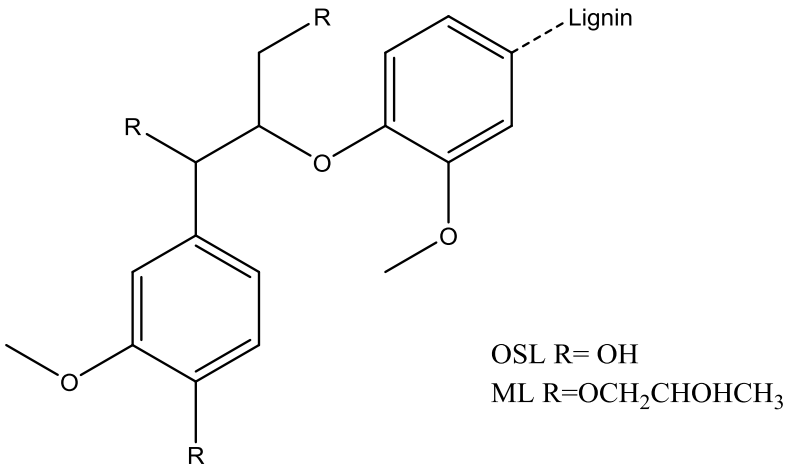

Figure 1. Simplified molecular structure of lignin used in this study.

2.2 Characterisation

Differential Scanning Calorimetry (DSC)

The glass transition temperature (T_g) of the two lignins were determined using Differential Scanning Calorimetry measurements (DSC 6, Perkin Elmer, USA) under a nitrogen flow at 60mL/min. The powder samples were compressed into 2 mm thick disks and dried in a vacuum oven for 24 hours at 60 ^{o}C. 15 ± 1 mg of sample were introduced in a sealed aluminium pan and heated to 150 ^{o}C at 10 ^{o}C/min to remove thermal history [20], cooled to 30 ^{o}C at 20^{o}C/min and reheated to 150 ^{o}C at a heating rate of 20 ^{o}C/min as described in (LISPERGUER et al. 2009). T_g was determined from the second heating curve.

Thermal Gravimetric Analysis (TGA)

The thermal stability of the lignins in air were characterised using a SETARAM TG-DTA 1600 (Setaram Instrumentation, France), using alumina crucibles. The samples were heated from 30 ^{o}C at a heating rate of 10 ^{o}C/min up to different temperatures (180 ^{o} and 200 ^{o}C). The temperature was held for one hour before cooling.

Fourier-transform infrared spectroscopy (FTIR)

Structural analysis of the samples before and after thermal treatment at three different temperatures (160 ^{o}, 180 ^{o} and 200 ^{o}C) for one hour was carried out using Fourier Transformed InfraRed (FTIR) transmission spectroscopy (Perkin Elmer Spectrum 100 FTIR Spectrometer, USA) in the ATR mode in the range of 4000-650 cm^{-1} with a 2 cm^{-1} resolution. Each spectrum was taken with 10 repetitions.

Thermal Gravimetric-Fourier transform infrared spectroscopy (TGA-FTIR)

Lignin samples were dried in vacuum oven at 80 °C for at least 8 hours before the analysis. Experiments were performed using TA Instruments SDT 2960 simultaneous DTA/TGA apparatus using a platinum pan under nitrogen flow (100 mL/min). The heating rate was set at 10 ºC/min and experiments were heated from room temperature to 1200 ºC. Exhaust gases from the TGA Instrument were collected inside a heated gas line (T=180 ºC) connected to a Thermo-Fischer Nicolet iS10 FTIR instrument. The collection of the series started at 50 ºC and FTIR spectra were recorded in absorbance units. To ensure an inert atmosphere, a similar ramp was performed without samples before every analysis. 3D graphs (absorbance, wavenumbers and time), FTIR spectra at temperatures of interest and concentrations of the identified substances water (3850 cm^{-1}), methane (3016 cm^{-1}), carbon dioxide (2360 cm^{-1}), carbon monoxide (2175 cm^{-1}), a carbonyl species (possibility acetone at 1738 cm^{-1}) and methanol (1032 cm^{-1}) and as functions of temperature (i.e. as Gram-Schmidt plots) were reported. The identification of gaseous compounds was realised through OMNICTM FTIR software.

UV-Difference Spectrophotometry

The number of phenolic groups was determined using the UV-Difference Spectrophotometry method before and after thermal treatment at 180 ^{o}C for one hour. The lignins were dissolved in ethylene glycol at a concentration of 10.0 g/L. They were then diluted in ultra-pure water to a concentration of 5.0 g/L. A buffer solution of pH=6 was prepared from phosphate salts, HPO_4^{2-} and $H_2PO_4^{-}$ (Sigma Aldrich). An alkaline solution of

0.2 M NaOH was prepared. 100 µL of each sample was diluted in 10.0 mL of each solution i.e. pH=6 and 0.2 M NaOH, to a final lignin concentration c = 0.05 g/L.

UV/Vis spectra were collected using Perkin Elmer Lambda 950 nm UV-Vis-NIR spectrophotometer, between 200 and 400 nm with a 0.5 nm interval and a speed of 133.4 nm/min. The quartz cuvette used has a path l = 1 cm. A pH=6 for each sample was used as a reference and the absorbance spectra for the super alkaline (A_2) was measured against it. The difference of absorption ΔA was measured at 300 nm and 360 nm. The concentration of phenolic hydroxyl groups was determined using the following formula (Zakis 1994; Gartner 1999) [21, 22].

$$Total\ OH_{ph} = \frac{0.250 \times \Delta A^{300\ \mathrm{nm}} + 0.107 \times \Delta A^{360\ \mathrm{nm}}}{l \times c} \quad (1)$$

Rheology

The rheological measurements were carried out in a Discovery Hybrid Rheometer (DHR-2) from TA Instruments using a parallel geometry with disposable aluminium plates (25 mm diameter plate). The experiments were carried out in isothermal mode for 3600 s at three different temperatures (160 º, 180 º and 200 ºC) using a shear rate of 10 rad/s. The lignin powder was placed between the plates. Then, the sample was heated until the desired experimental temperature leaving a gap of 1 mm between plates.

The cross-linking kinetics were analysed using chrono-rheological data according to the following equations [19]:

$$\ln \eta(t) = \ln \eta_{\gamma} + kt \quad (2)$$

$$\eta_\gamma = \eta_\infty e^{\frac{\Delta E_\eta}{RT}} \quad (3)$$

$$k = k_\infty e^{\frac{\Delta E_k}{RT}} \quad (4)$$

where k is the temperature dependent reaction rate constant, k_∞ is the equilibrium rate constant, η_∞ is the viscosity at infinite shear rate, η_γ is steady viscosity value at the onset of viscosity rise, ΔE_η and ΔE_k are the activation energies associated with the temperature dependence of the steady viscosity and the rate constant, respectively.

Dielectric Relaxation Spectroscopy (DRS)

Dielectric experiments were performed in a liquid parallel plate sample cell (BDS1308). The electrode gap was adjusted by silica spacers. The measurements were carried out in the temperature range from 90 º to 230 ºC (at steps of 5 ºC) and a frequency window of 4.9×10^{-2} to 1×10^{6} Hz using a Novocontrol BDS system comprising a frequency response analyser (Solartron Schlumberger FRA 1260) and a broad-band dielectric converter with an active sample head. The measurement error was shown to be less than ±3%.

Some authors have reported the interesting use of dielectric properties to monitor the progress of reactions in different polymeric systems [23-26]. The dielectric response of a substance is commonly presented as complex permittivity (ε^*), which can be given by

$$\varepsilon^*(\omega,T) = \varepsilon'(\omega,T) - j\cdot\varepsilon''(\omega,T) \quad (5)$$

where $\varepsilon'(\omega, T)$ represent the real part, generally known as dielectric constant (a measure of the ability of the material to store electrical energy), $\varepsilon''(\omega, T)$ represent the imaginary part, also called the dielectric loss factor (a measure how the energy is dissipated or lost), $\omega=2\pi f$ is the angular frequency and j ($j^2=-1$) is the imaginary unit. The ratio of loss factor to the dielectric constant, called the tangent loss ($\tan\delta=\varepsilon''/\varepsilon'$) enabling, among others, to estimate the material's ability to convert electromagnetic energy into heat at a specific temperature and frequency [27]. In this vein, lignin derivatives are considered to be low loss dielectric materials which mean they do not absorb microwave energy well [28-30].

In order to characterize the conductive behavior, the obtained dielectric data are represented in terms of dielectric constants such as: (i) dielectric modulus $M^*(\omega)=1/\varepsilon^*(\omega)$, and complex conductivity parameters $\sigma^*(\omega)$. $\varepsilon^*(\omega)$ and $\sigma^*(\omega)$ which are related to each other by $\sigma^*(\omega) = \sigma'(\omega) + j\sigma''(\omega) = i\omega\varepsilon_0\varepsilon^*(\omega)$, where $\varepsilon_0=8.85\cdot10^{-12}$ F·m^{-1} is the vacuum permittivity. So, the real and imaginary parts of $\sigma^*(\omega)$ are given, respectively, by $\sigma'(\omega) = \sigma'_{ac}(\omega) = \omega\varepsilon_0\varepsilon''(\omega)$ and $\sigma''(\omega) = \omega\varepsilon_0\varepsilon'(\omega)$. In general, the ac conductivity, $\sigma'(\omega)$, at a constant temperature can be represented by $\sigma'(\omega)= \sigma_{dc} + A\omega^s$, where σ_{dc} is the independent frequency conductivity or dc conductivity (at $\omega\rightarrow0$) and the A and s parameters are constants dependent on temperature.

3. Results and discussion

According to DSC results, both lignins, OSL and ML, display thermoplastic behaviour with a T_g of 100 º and 115 ºC respectively, as shown in **Figure 2**. The absence of melting point indicates the amorphous nature of OSL and ML. The difference in T_g values is

attributed to the molecular weight and the associated differences in molecular entanglements between the polymer chains of each kind of lignin.

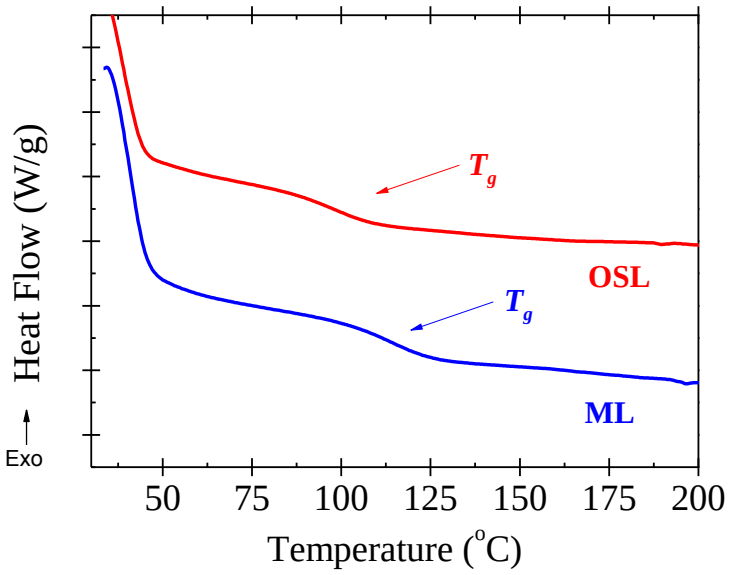

Figure 2. DSC curves of lignin samples (OSL and ML).

As would be expected the modified lignin, with its higher molecular weight, shows the higher T_g value. The rather diffuse nature of the transition is, in both cases, a function of the high degree of polydispersity. There is no evidence of secondary sub-T_g relaxations in either of the plots, although such events must be possible in the modified lignin through crankshaft rotation of the hydroxypropyl arms. [31] It is possible that such events occur below the start temperature of the experiment.

Thermochemical behaviour: Coupled TGA-FTIR analysis showed that both lignins exhibited a release of water, carbon dioxide and carbon monoxide as the temperature rises above 200 ºC, equivalent to a heating time of 20 min (**Figures S2**(a) and (b)), and evolution of carbon dioxide continues throughout the entire run rising to maximum levels above 1100 ºC. These trends are seen more clearly as Gram-Schmidt plots in **Figures 3**(a) and (b).

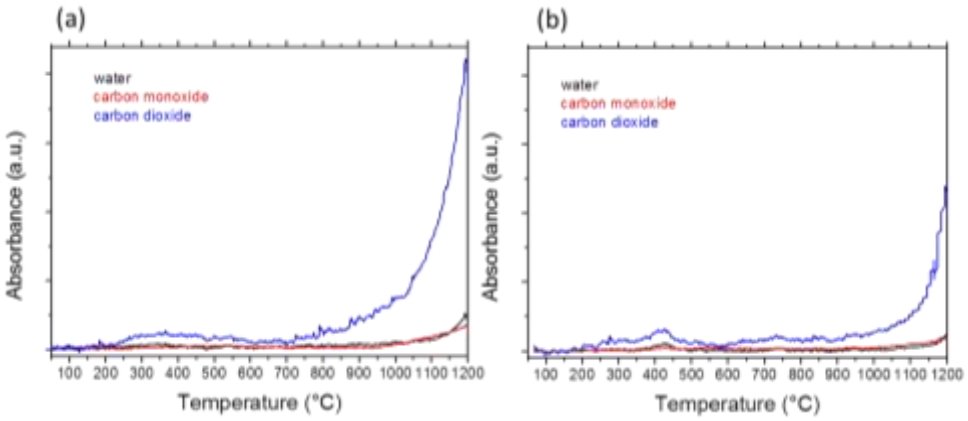

Figure 3. Gram-Schmidt plots of (a) OSL and (b) ML for water (black), carbon monoxide (red) and carbon dioxide (blue).

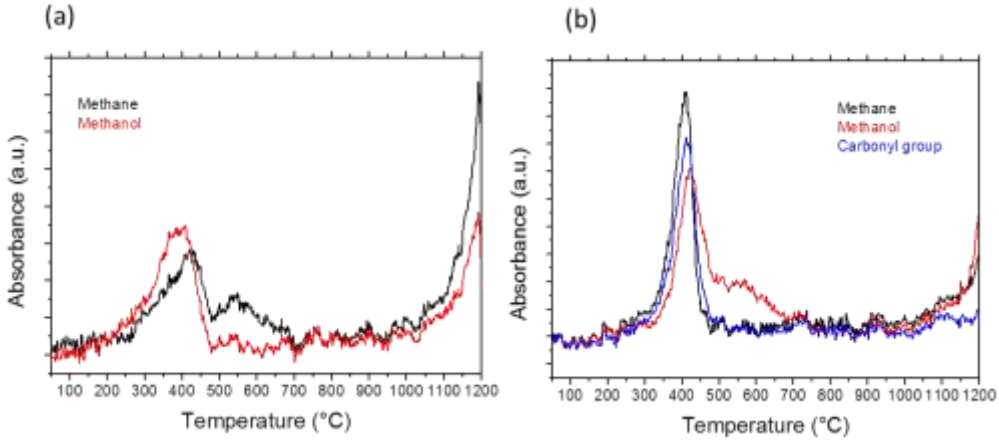

Figure 4. Gram-Schmidt plots of (a) OSL and (b) ML for methane (black), methanol (red) and carbonyl group (blue).

Methane and methanol were also detected for both lignins with maxima occurring in the 350-400 ºC range as shown in **Figures** 4(a) and (b). In the case of OSL, the release of both methane and methanol started at ~200 °C, with respective maxima at 400 °C for methanol and at 435°C for methane. While evolution of methanol completed by about 480 °C, methane exhibited another evolution peak at ~ 550 °C decaying gradually until ~700 °C. ML, showed more intense emissions of both methane and methanol than OSL, maximising

again at ~ 400^{o}C, with only methane showing a higher temperature peak as a shoulder at ~ 550^{o}C. The carbonyl peak evolution in **Figure 4**(b), is considered to be associated with acetone, presumably a result of scission of the hydroxypropyl substituent present in lignin ML (see **Figure 1**).

The isothermal thermograms under nitrogen of OSL and ML at 180 ºC and 200 ºC after water loss are shown in **Figure 5**. ML showed higher thermal stability at both temperatures compared to OSL. The modified lignin, ML, lost 0.43 and 0.59 % of its weight at 180 º and 200 ºC, respectively, while OSL lost 0.88 and 1.7 % at 180 º and 200 ºC, respectively after 1 hour.

According to the TGA-FTIR data the weight lost associated with the isothermal treatment at 180 º and 200 ºC for both lignins can be attributed partly to the release of carbon dioxide since this is the major gas formed as the temperature rises above the latter (see **Figure 3**). However, for the case of OSL the weight lost at 200 ºC treatment can also be attributed to the release of methanol since its evolution begins just below this temperature (see **Figure 4(a)**).

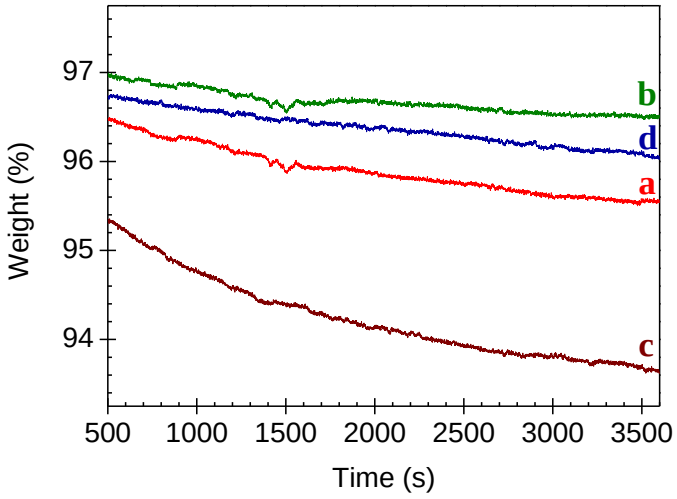

Figure 5. Weight loss as a function the time at 180 ºC for OSL(a) and ML(b) and at 200 ºC for OSL (c) and ML(d).

Figure 6 (a) shows complete ATR mode FTIR spectra of both lignins as received and in Figures 6(b) and (c) respectively after heat treatment at 160 º, 180 º and 200 ºC for 1 hour over the range 1400-1200 cm^{-1}. Both spectra in **Figure 6(a)** present typical features for lignin. At 1595, 1510 and 1420 cm^{-1} appear resonances bands caused by the aromatic skeletal vibrations, principally the aromatic C–H in plane and out-of-plane as well as the C–H deformation combined with aromatic ring vibration at 1455 cm^{-1} for both lignins showing that the hydroxypropyl modification of ML did not affect the phenyl structure.

The aromatic overtone bands, diagnostic of the type of substitution, are similar with both lignins before heat treatment confirming the skeletal similarity. The spectral differences lie almost entirely in the aliphatic region with the methyl and ethyl ratios influencing the sub-3000cm^{-1} peaks and 1000 cm^{-1} to 1500 cm^{-1} region.

The broad resonance with a maximum at 3400 cm^{-1} is attributed to the stretching of O–H groups in phenolic and aliphatic structures. Phenolic hydroxyl groups resonate weakly at 1370 cm^{-1} [31], although the effect is more marked for OSL than ML (see **Figures 6 (b)** and

(c)), which corroborates the results obtained in UV-Difference analysis summarized in **Table1** and the results observed in ^{13}C-NMR analysis shown in **Figure S4**. The C–H stretch frequencies typical of methyl and methylene groups are present in both spectra with characteristic vibrations at 2930 cm^{-1}.

Table 1. Phenolic hydroxyl contents in OSL and ML lignins determined via UV-Difference Method (The samples heat treated at 200 ºC were not analysed as the solids would not dissolve in ethylene glycol).

	OSL as received	**OSL at 180 ºC**	**OSL at 200 ºC**	**ML as received**	**ML at 180 ºC**	**ML at 200 ºC**
OH_{Ph} (mmol/g)	2.4	3.4	-	0.33	0.35	-

Finally, the presence of conjugated aldehydes and carboxylic acids is shown by a resonance below 1700 cm^{-1} (see **Figure 6 (a)**). Bands at 1330–1328 cm^{-1} and at 1270–1262 cm^{-1} represent C–O stretching in the Syringyl (S) and Guaiacyl (G) rings, respectively. The characteristic vibrations for G are strong in ML (1262 cm^{-1} for G ring stretch, C–H in plane deformation at 1138 cm^{-1} and C–H out-of-plane vibrations at 857 cm^{-1}). In OSL are present the typical resonances of C–O stretching of S units, at 1326 cm^{-1} and C–H in plane deformation at 1112 cm^{-1}. In addition, ML shows a more intense band centred at 1020 cm^{-1} that is attributed to the C–O deformation of secondary alcohols due to the hydroxypropyl modification.

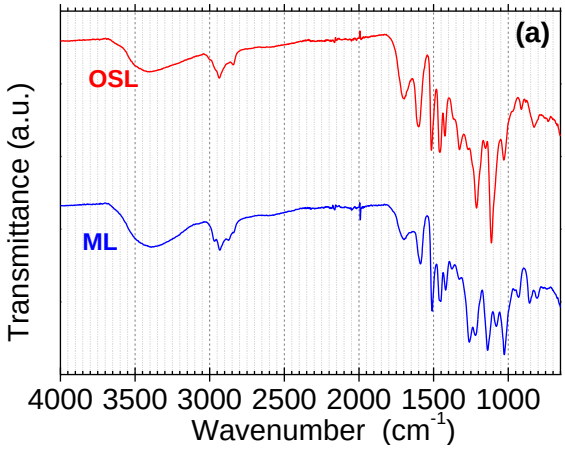
(a)
OSL
ML
Transmittance (a.u.)
4000 3500 3000 2500 2000 1500 1000
Wavenumber (cm-1)

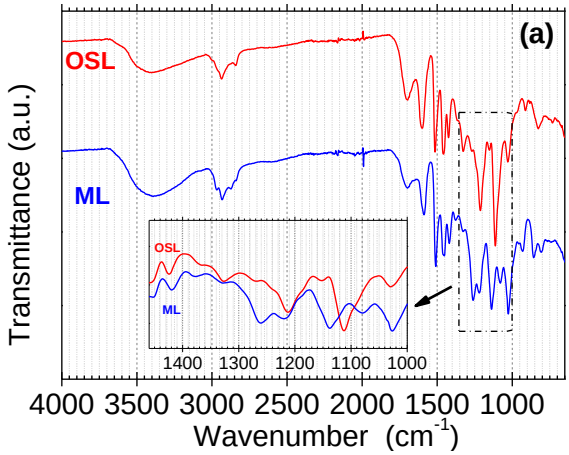
(a)
OSL
ML
OSL
ML
1400 1300 1200 1100 1000
Transmittance (a.u.)
4000 3500 3000 2500 2000 1500 1000
Wavenumber (cm-1)

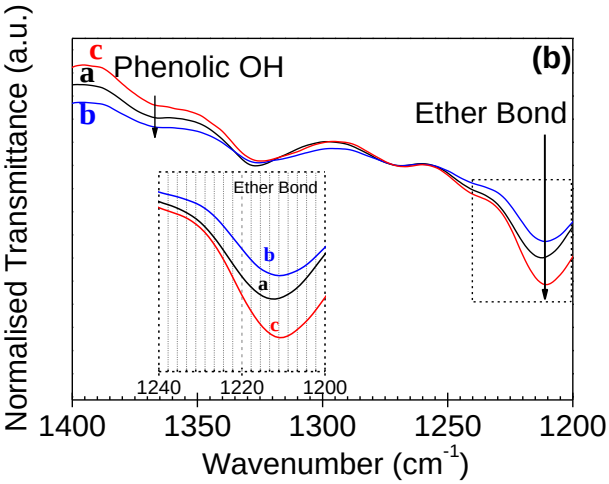
(b)
c
a
b
Phenolic OH
Ether Bond
Ether Bond
b
a
c
1240 1220 1200
Normalised Transmittance (a.u.)
1400 1350 1300 1250 1200
Wavenumber (cm-1)

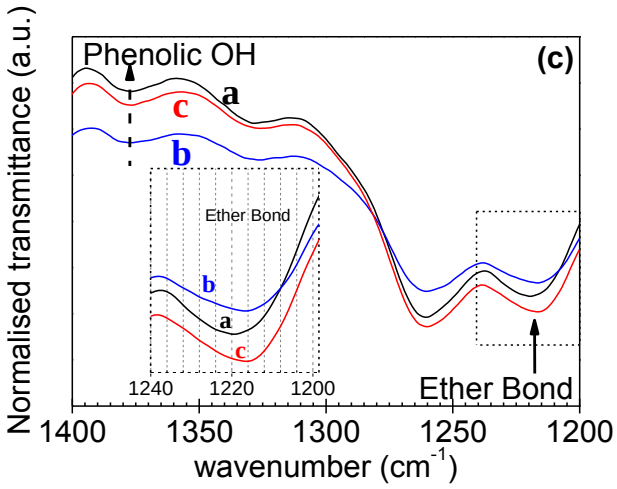

Figure 6. FT-IR spectra of (a) the as received lignins, (b) OSL after heat treatment and (c) ML after heat treatment. (b) and (c) were normalised against the transmittance of the aromatic skeleton vibration at 1514 cm^{-1} (b) and 1509 cm^{-1} (c) as described in [19]. [Isotherm: **a**: 160 ºC, **b**: 180 ºC and **c**: 200ºC]

The heat treated sample spectra were analysed semi-quantitatively [19]. The aromatic skeleton vibration at 1515 cm^{-1} was considered unchanged during the heat treatment, it was therefore used to normalise the signals of all the samples, as can be observed in **Figures 6(b)** and **(c)**. However, according to the FTIR results, the chemical composition influences the intensity and energy of the ether bond absorption band, but also the transmittance ratio between the bands associated with the phenolic OH and ether bond (**Figures 6(b) and (c)**). The absorption maxima of the ether bond band shifted to lower energy wavenumbers when degradation temperature increased. Thus, ether bond absorption maxima of both OSL and ML samples, observed at 1213 cm^{-1} and 1220 cm^{-1}, were shifted to 1211 cm^{-1} and 1217 cm^{-1} by increasing the temperature to 180º or 200ºC. These shifts can be linked to crosslinking and structural modification with increasing temperature [31] and this correlates with the rheological findings summarized below. The FTIR for both lignins and the UV

Difference method results in **Table 1** for OSL show that at 180 ^{o}C, the amount of ether linkage decreases as the phenolic hydroxyl group content increases which suggests the degradation of ether groups into phenolic hydroxyl groups as previously reported [19] and was evidenced in the TGA-FTIR analysis here. However, the phenomenon is reversed at 200 ^{o}C, as cross-linking is thermally favourable at higher temperatures in these systems. In addition, this change is greater in OSL indicating that this lignin favours thermally induced crosslinking reactions.

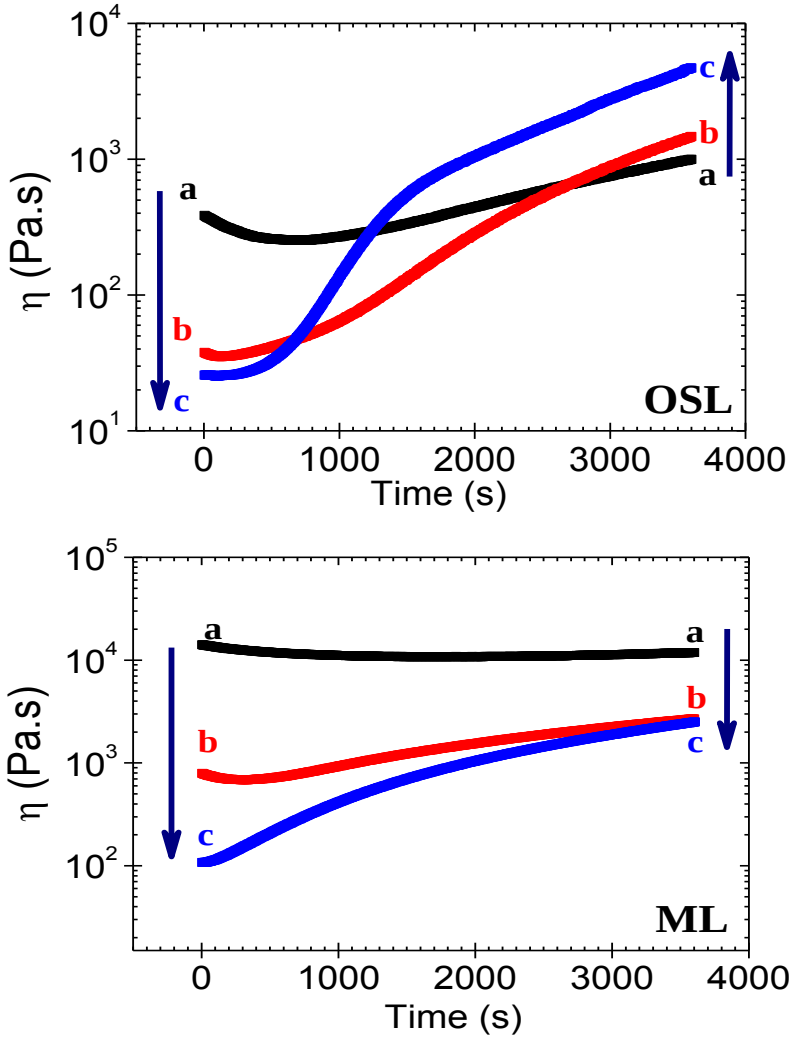

Figure 7. Viscosity as function of the time at 160 º [a], 180 º [b] and 200 ºC [c] of OSL and ML. Arrows mark the temperature increase direction.

To quantify the flow behaviour of the samples (OSL and ML), changes in the steady shear viscosity, η, were measured as a function of time at three selected temperatures (160 º, 180 º and 200 ºC) (see **Figure 7**). Both systems were characterised by an increase in the steady shear viscosity during the heating time, and such behaviour is common to this generic group [19]. In analysing these results there are two factors to be considered: first the increased molecular mobility consequent upon the higher molecular energy, and secondly the tendency of the components to undergo intra and inter-molecular rearrangement thereby changing the distribution of molecular sizes and molecular polarity through hydrogen bond change [19,32]. Within the time scale of the experiment the dominant effect with the modified lignin is that of temperature induced viscosity reduction with a smaller viscosity increase contribution from molecular rearrangement, whereas with the OSL material viscosity increase through crosslinking is clearly the dominant effect. These viscosity observations are fully consistent with the isothermal thermogravimetric curves, shown as **Figure 5**, where the OSL is losing mass at approximately twice the rate of the ML.

The time dependence of the viscosity was analysed using the isothermal viscosity data shown in **Figure 7**. **Table 2** shows the values of k_∞, η_∞ $\Delta E_\eta/R$ and $\Delta E_k/R$ fit parameters for both lignins. The activation energy for the rate constant ($\Delta E_k/R$) and for the thermal reactions ($\Delta E_\eta/R$) are higher for ML lignin. This different behaviour derives from their different molecular structure is considered to arise from the greater molecular mass of the ML material and the added complexity of the crosslinking reactions, which must involve additional steps when compared with the OSL material.

Table 2. The fit kinetics parameters of lignin samples analysed.

Lignin	$\Delta E_k/R$(K)	$\Delta E_\eta/R$(K)	k_∞, s^{-1}	η_∞ (Pa·s)
OSL	-1464.0	2615.0	4.8	$1.01 \cdot 10^{-5}$
ML	-2315.8	3584.6	174.1	$1.64 \cdot 10^{-6}$

Figure 8 shows the time dependence of the storage (G') and loss modulus (G'') of both lignins at the three different temperatures. For the case of OSL the loss modulus is higher than the storage modulus at 160 º and 180 ºC during the whole experiment indicating that the sample is behaving principally as a fluid material. In order to appreciate the combined effect of time and temperature on the stiffness of the OSL sample, we have plotted in the inset of **Figure 8a** the temperature dependence of the storage modulus for t = 0s and t = 3600s. At short times G' slightly decreases between 160 ºC and 200 ºC, whereas a long times G' increases significantly indicating that the material becomes stiffer. However, there is a crossover at 2700 s when the temperature of the experiment was 200 ºC probably due to the onset of cross-linking as discussed in the rheology section. New inter-unit linkages are created when the OSL sample reaches sufficient internal molecular mobility. However, for the case of ML there is a crossover at 1500 s indicating that OSL has a slower onset point for cross-linking reactions to initiate. This is attributed to the higher degree of branching in ML which allows the faster onset of cross-linking when compared to OSL, according to the molecular weight values and DSC analysis. Isothermal TGA results (**Figure 5**), show a relatively low weight losses for both lignins, indicating that probably, the changes in the rheological behaviour are primarily generated by polymerizations and de-polymerization reactions in lignin polymer chains.

At all temperatures both lignins behave predominantly as fluids with the loss modulus exceeding the storage modulus, although at the higher temperatures the stiffening effect of the crosslinking reactions is becoming more apparent. The overall mechanical stiffness of the ML material is apparent at all three temperatures and is explained through molecular mass causing hindrance to motion. These dynamic mechanical results correlate well with the viscosity observations previously described. In both cases ML lignin shows greater thermal stability at the lower temperature and a slower rate of property change as temperature of observation is increased. In the inset of **Figure 8b** by increasing the temperature between 160ºC to 180ºC a reduction of *G´* is observed over long time periods, whereas a clear increase between 180º and 200ºC is produced. This may reflect the multi-step degradation and crosslinking process of this material. The thermogravimetric results, presented as **Figure 5**, provide further support for this interpretation where it is observed that over the temperature range considered the weight loss of the ML lignin is consistently lower than that of the OSL material.

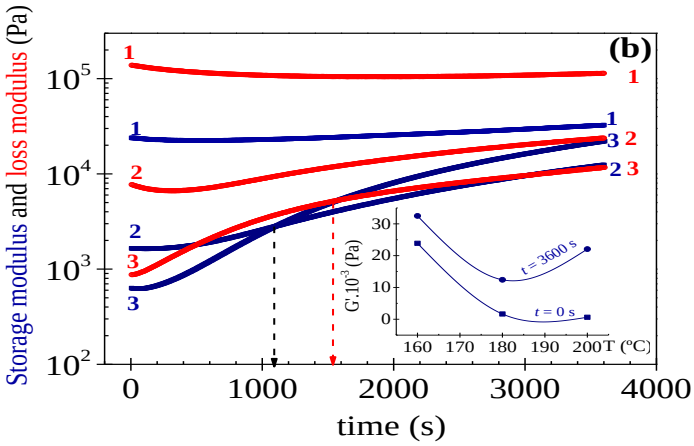

Figure 8. Storage and loss modulus as a function of the time at **1**:160 º, **2**:180 º and **3**: 200 ºC for (a) OSL and (b) ML. Inset: Temperature dependence of the storage modulus at lower and higher times.

The dielectric properties of both lignin samples were determined from 90 ºC to 230 ºC (step 5ºC) at forty-seven different frequencies between 10^{-2} Hz and 10^{6} Hz. In order to describe the general temperature dependence tendencies of the dielectric properties, as an example, results are shown for 10^{5}Hz in **Figure 9.**

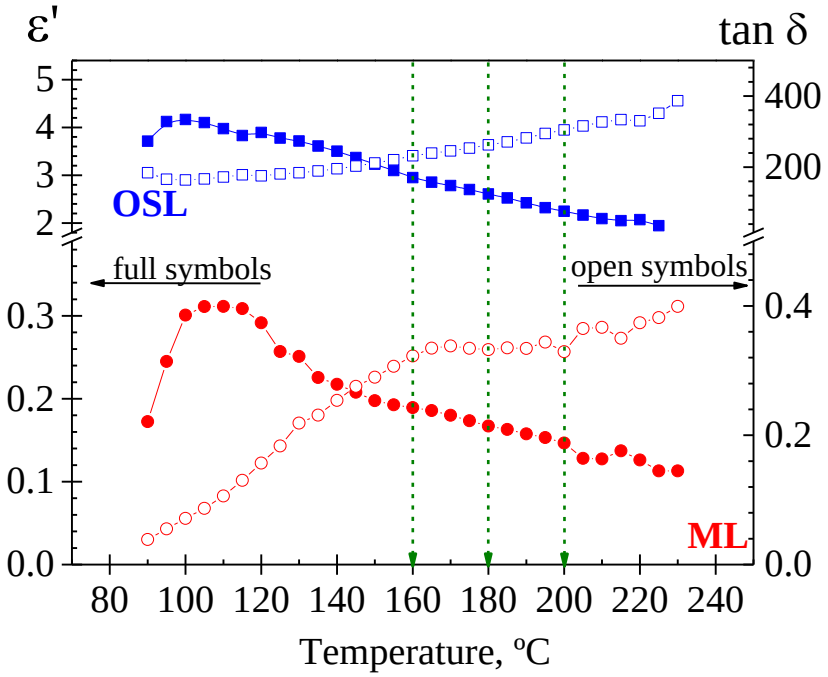

Figure 9. Temperature dependence of dielectric permittivity (full symbols) and loss tangent (open symbols) for OSL (square) and ML (circle) at a frequency of 10^{5}Hz.

The values of dielectric constant (ε') and loss tangent (tan $\delta=\varepsilon''/\varepsilon'$) for both samples (OSL and ML) displayed a similar profile, and is in close agreement with other biomass materials [30, 33, 34]. The absolute values of dielectric constant and tan δ are different for the two lignins, reflecting the differences in polarizability and these differences are maintained as temperature is increased. Both dielectric variables present higher values for OSL than for ML. Dielectric constant spectra show an event shortly after heating begins, related in both

cases to loss of water. Then, the dielectric constant reduces upon moisture removal. This suggests that the dielectric constant is directly related to the presence of free and/or bound water. The dielectric constant varies between 2 and 4.2 for the OSL sample and between 0.14 and 0.32 for the ML sample. As the dielectric constant depends strongly on the molecular structure (e.g. flexibility, functionality) of the sample, the lower values obtained for ML can be related to (i) the lower primary hydroxyls content as a result of the lignin modification and (ii) the lower strength of solid-water interactions in this lignin. On the other hand, the reduction of the dielectric permittivity values as temperature increases can be attributed to the release of surface and weakly bound water molecules from the sample. This causes a gradual decrease in dipole movement or change in its orientation. The polymer chains become restricted in movement, which results in a decrease in the dielectric constant. In this sense, it is important to highlight that the lignin-water hydrogen bonds are broken more easily when compared to lignin-lignin hydrogen bonds. [31,35] On the other hand, the decrease of dielectric properties between 180 ºC to 230 ºC can be assigned to the partial decomposition of lignin and/or formation of new inter-unit linkages produced when lignin reaches sufficient internal mobility. Thus, at high temperature, lignin segments have a sufficient degree of freedom to allow cross-linking reactions to take place. [31] As a result, these new inter-chain linkages increase the rigidity of lignin, through a reduction in chain mobility. These microstructural changes are directly related to the increase of viscosity at macroscopic scale as detailed above and shown in our IR, UV and TGA results. On the other hand, for the ML sample, the tangent loss exhibits lower values ($\tan \delta < 0.04$) over the whole range of frequencies, which is indicative of electrical insulating properties. The static T_g results, from DSC, show that the glass transition temperature occurs at 100 ºC

approx. (OL) and 115º C approx. (ML) but an equivalent event is not apparent in the loss tangent plots as a consequence of the strong conductivity contribution to the loss permittivity (as a result, tan δ). At higher temperatures and lower frequencies, above the glass transition temperature, the dielectric spectra are dominated by conductive processes. These are related to the extrinsic migrating charges (e.g. ionic impurities remaining from synthesis steps) and intrinsic migrating charges (e.g. proton transfers along hydrogen bonds) [27]. While it is expected that extrinsic migrating charge contributions decrease as a result of an increase in viscosity, the intrinsic migrating charges may follow a more complex pattern. That is why as viscosity increases, the overall conductivity can follow different behaviours depending on which mechanism (extrinsic or intrinsic) is dominant in the dielectric response[23, 27 37-39].

The ε^* data were accordingly transformed into M^* to analyse the conductivity process for both lignin samples. In **Figure 10** the frequency dependence of the dielectric loss modulus, M'' ($M''=\varepsilon''/(\varepsilon'^2+\varepsilon''^2)$) at the three chosen temperatures (160 º, 180 º and 200 ºC) are plotted. In view of the T_g established by DSC, the absorption present in these spectra are related to the conductive process. For both lignin samples, the higher the temperature, the greater intensity of the maximum. However, with respect to the frequency/temperature dependence of the loss modulus, significant differences between both samples are observed, as a consequence of the initial structural differences and of the possible redistribution of bonds, as well as formation of new interunit linkages favoured by changing the temperature and time conditions. So, whereas the maximum loss modulus peak shows a shift towards higher frequencies (lower times), as usual, for the OSL sample, the frequency of the maximum does not change significantly for the ML sample. This result

confirms again that a different structural change is produced in both samples as the temperature increases. On the other hand, as the temperature increases, a broader distribution of the peak associated with the conductive process is observed, indicating a greater heterogeneity.

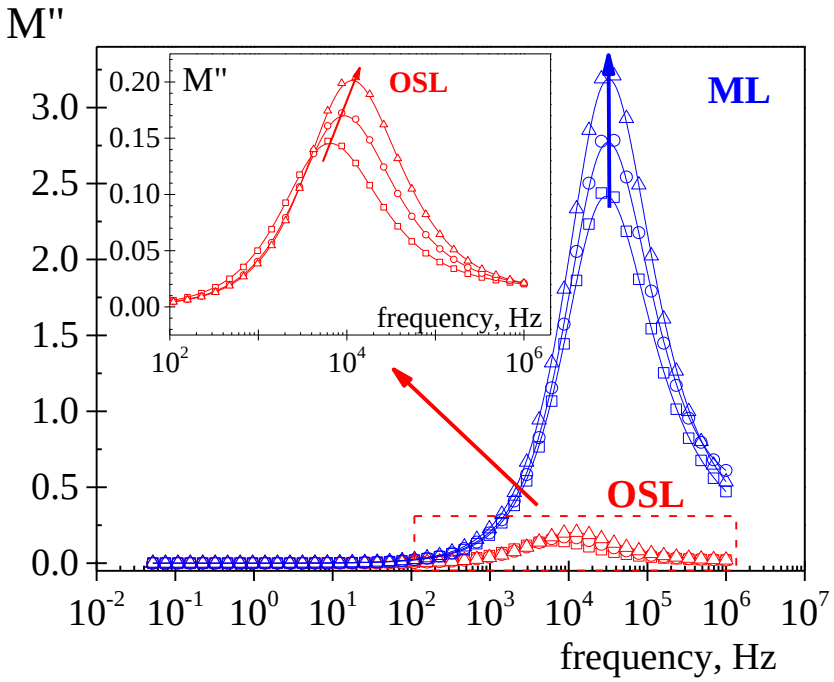

Figure 10. Frequency dependence of the loss modulus at 160 ºC (square), 180 ºC (circle) and 200 ºC (triangle) for both OSL and ML lignin samples. Arrows mark the temperature increase direction.

Also, to analyse the conductivity properties of the lignin samples it is useful to express the experimental measurements using the complex conductivity, related to the permittivity as $\sigma^*(\omega) = i\omega e_0 \varepsilon^*(\omega)$, where e_0 (8.854 $pF \cdot m^{-1}$) is the dielectric permittivity of the empty space. **Figure 11** shows a double logarithmic plot of the frequency dependence of the real component of the complex conductivity, $\sigma'(\omega) = \sigma'_{ac}(\omega)$, measured at 160 ºC, 180 ºC and

200 ºC, for both OSL and ML lignin samples. According to our results, the incorporation of additional hydroxypropyl units in the molecular chain in ML has disrupted ionic conductivity compared to OSL. This behaviour could be related to the higher initial cross-linking degree of the native ML material, which would hinder the charge motion. Additionally, the structural changes taking place in the lignin samples promote opposite tendencies in the temperature dependence of conductivity. Whereas, the conductivity increases with the temperature for the OSL sample, a reduction with temperature is observed for the ML sample. In order to clarify the observed trends, in the inset of **Figure 11** we have plotted the frequency dependence of the imaginary part of the impedance taking into account the relationship between both dielectric constants: $\sigma^*(\omega) = \varepsilon_0 / \left[C_0 \cdot Z^*(\omega) \right]$. Thus, for the OSL sample, the imaginary impedance peak (Z''_{max}) shifts to higher frequency and lower impedance by increasing temperature. This trend means that by increasing temperature the resistivity of the system decreases. However, for the ML sample, the imaginary impedance peak shifts to lower frequency and higher impedance, consequently the conductivity decreases. What is the mechanism that causes the opposite trends in conductivity? The answer possibly lies in the fact that intrinsic conductivity, relates to the inherent chemical characteristic of the material, which depends on the availability of proton transfers along hydrogen bonds. So, in the case of OSL, the chemical change produced, when temperature increases, promotes the cross-linking between adjacent benzene rings with the consequent rise in conductivity. On the other hand, the changes shown for ML samples may be associated with the formation of less conductive species, thereby inhibiting charge transport (see **Figure 12**). This decrease in conductivity accompanied by an decrease in viscosity has also been observed in other reactive systems [40]. These opposite

tendencies, for both analyzed samples, were consistent with the time dependence of the viscosity and shear modulus for long times (low frequencies).

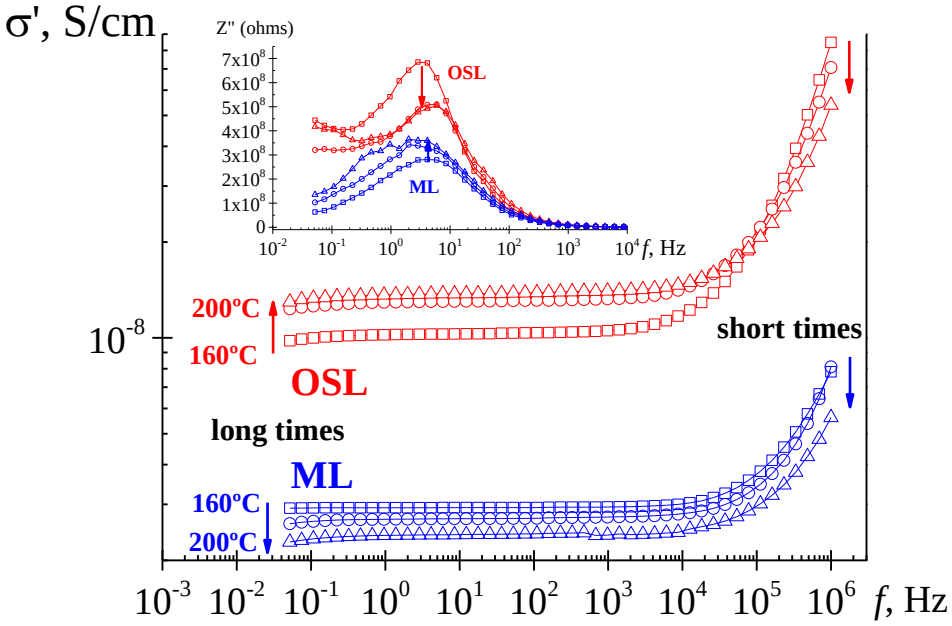

Figure 11. Frequency dependence of the conductivity at 160 ºC (square), 180 ºC (circle) and 200 ºC (triangle) for both OLS and ML lignin samples. Inset: frequency dependence of the imaginary part of the impedance. Arrows mark the temperature increase direction.

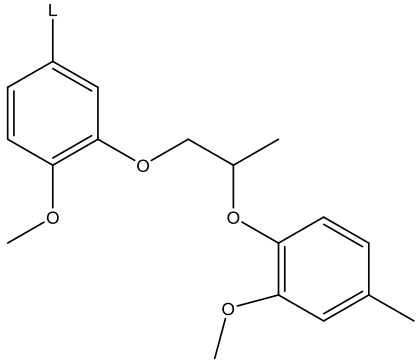

Figure 12. Scheme of the proposed linkage in ML lignin.

Figure 13 shows the temperature dependence of the dc conductivity, evaluated from the plateau value of the isotherms (see **Figure 11**). At least two regions are evidenced in this figure. In the lower temperature region, it is observed that the temperature dependence of dc conductivity for both samples is similar. At about 120 ºC, a significant change in the slope is observed for both samples. For ML, even a positive slope is observed for temperatures higher than 175 ºC. The activation energy for conduction, for both regions, was obtained using the Arrhenius relationship (ln $\sigma_{dc}=A- E_a/RT$). At low temperature, near the glass transition temperature, the slope of the linear least- squares- fit of the conductivity data (**Figure 13**) provides us the following values for the apparent activation energy, E_a, for both lignins: 180.95±9.09 for OSL and 156.07±13.95 kJ/mol for ML. At higher temperatures the activation energy evaluated from the slope of the plot was as the same magnitude order as those summarized in **Table 2**. The conductive activation energy decreases with increasing temperature as a consequence of the chemical changes during processing.

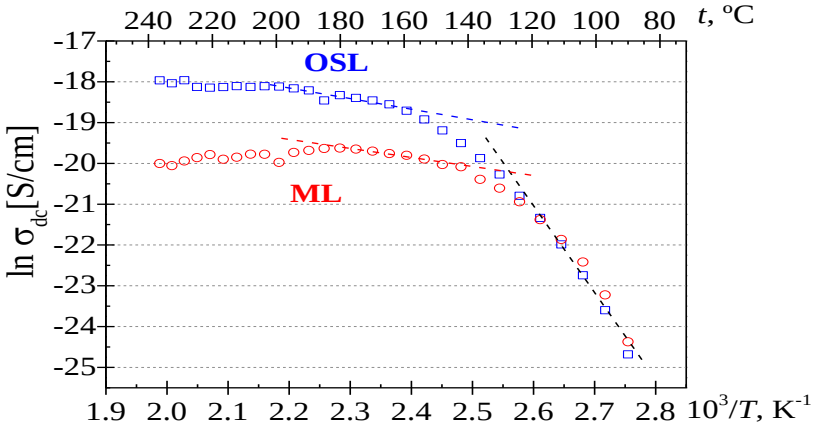

Figure 13. Temperature dependence of dc conductivity for both OLS and ML lignin samples.

The transport properties such as conductivity and shear viscosity are crucial properties for the practical use of the materials. For this reason, several correlations between measured conductivity and other processing parameters, such as viscosity have been established. [41-45] To facilitate the interpretation of results, in **Figure 14,** the temperature dependence of the ac and dc (inset) conductivity and the complex viscosity are plotted. This figure shows clearly the correlation between the decreasing conductivity and the increasing viscosity. This tendency is related to the decrease in the ability of charge to diffuse through an increasing viscous medium, according to the Stokes-Einstein equation. On the other hand, the conductivity is directly proportional to the diffusion coefficient of the mobile species through the Nernst-Einstein equation. Therefore, both conductivity and viscosity are inversely related. For both samples, up to 160ºC, the ac conductivity increases sigmoidally with increasing temperature, noting again the possible existence of two different conduction mechanisms. Thus, for OSL sample, the conductivity rises markedly with increasing temperature and the temperature dependence of the complex viscosity follows the opposite trend to the ac conductivity, showing a minimum and maximum, respectively, at 190ºC approx. However, for the ML sample, a nearly temperature independent conductivity in the initial mixture from 160ºC is a result of the commensurate effect of temperature on intrinsic conductivity (which probably decreases with increasing temperature as the hydrogen-bonding intensity does) and extrinsic conductivity (which increases with increasing temperature). Furthermore for this modified lignin sample, the conduction process is decoupled from that of viscous flow. Thus, the conductivity reaches the higher value at 170ºC approx., whereas the minimum of the complex viscosity is at 210ºC approx. This

result suggests that both temperature and time play a significant role in the crosslinking processes.

Taking into account that the principal contribution to the intrinsic conductivity in the systems studied is presumably from the hydrogen bonds between hydroxyl groups, and this contribution depends on the extent that those are blocked. The coupling/decoupling between conductivity and viscosity response by increasing temperature, shown for the OSL/ML samples, presents a new route for tailoring the macroscopic properties of these materials.

Thus, the viscosity changes of analyzed samples are essentially due to the competing effects of thermodynamic and kinetic factors. Increasing the temperature, the molecular mobility is raised and the viscosity decreases as expected. Increasing the exposure time at high temperatures, for OSL sample, the molecular mobility is reduced as a consequence of the crosslinking process, which leads to an increase of the viscosity, whereas for ML sample, a reduction of viscosity was observed. In the case of ML the effect of reaction temperature is the most critical factor, whereas for OSL the effect of the reaction time factor appears to be dominant. This result is in agreement with the kinetic parameters summarized in **Table 2**.

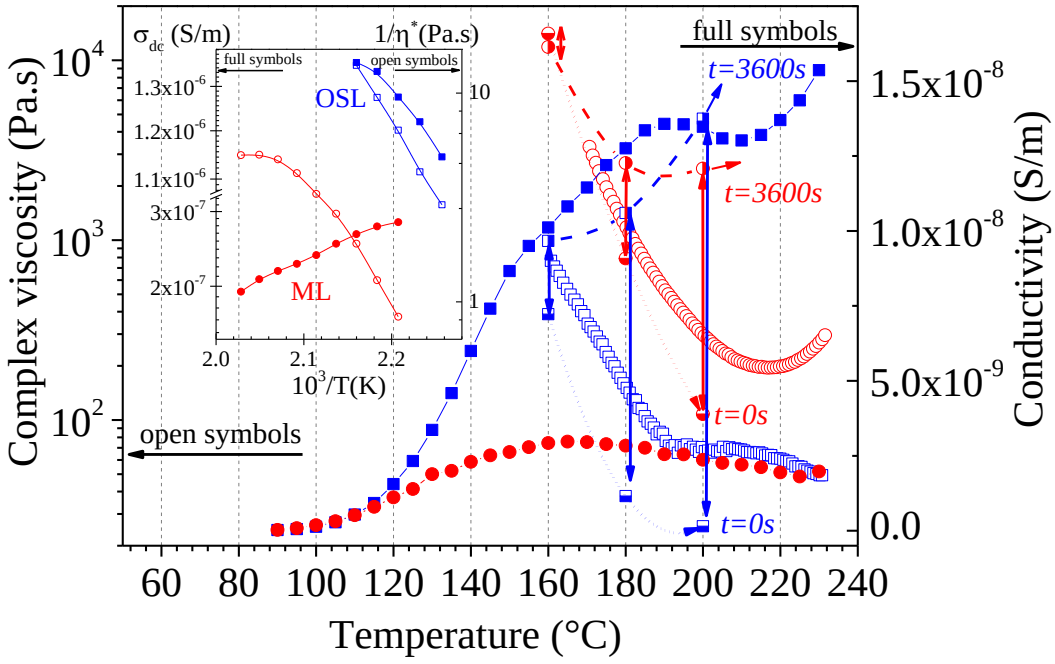

Figure 14. Temperature dependence of the complex viscosity (open symbols) and ac conductivity full symbols for OSL (square) and ML (circle) samples. The values of the steady shear viscosity for t=0 (⬓, ◒) and t=3600s (◨, ◑) for OSL and ML, respectively, are plotted also. Inset: Temperature dependence of σ_{dc} (full symbols) and $1/\eta^*$(open symbols).

Conclusions

The two lignins examined in this study, organosolv (OSL) and chemically modifies kraft lignin (ML), represent important classes of a potentially useful and abundant raw material and the analysis and comparison has concentrated on their utility as a starting polymer for the production of carbon fibre. For this application thermal characterisation and understanding of the thermo- mechanical degradation behaviour are critical.

Scanning calorimetry has shown that both materials are glassy and pass through the glass transition between 100 °C and 115 °C, with the higher molecular weight modified material having the slightly higher T_g. Low temperature isothermal stability, measured at180 °C and 200°C, of the modified lignin (ML) is greater than that of the organosolv (OSL) and this is consistent with the relative starting structures. At these lower temperatures (near T_g) the contribution of absorbed water has to be considered and dielectric relaxation results do suggest a continuing loss of moisture from the ML material at temperatures up to 110°C. The initial structural differences between the two lignins are very apparent in the dielectric constants, with the much higher dielectric constant values of the OSL reflecting the ready polarizability of the phenolic hydroxyl.

The rheological results, generated through low temperature isothermal heating, have been interpreted in terms of the competitive processes of thermal plasticization and stiffening through crosslinking. The results show that with OSL crosslinking proceeds relatively rapidly, and again this is consistent with the more reactive structure, as demonstrated by the previously mentioned thermogravimetry results. Activation energies, for flow and for reaction, calculated by application of Arrhenius type relationships give values similar to those obtained by previous workers and their relative magnitudes are consistent with the higher reactivity of the OSL.

The thermomechanical results further demonstrate for both materials, through rate of stiffness change, the progressive conversion of predominantly fluid systems to crosslinked solids, with the OSL again showing a much greater temperature sensitivity. At lower temperatures the ML material is consistently thermo-mechanically more stable. In both cases slight increases in phenolic hydroxyl concentrations occur on initial heating, though

this effect is small with the ML material and so this is thought to reflect the first stages of the crosslinking reaction. Importantly the spectral characterisation of the partially degraded materials suggests that there are differences in the detail of the crosslinking processes.

Continued heating, to temperatures up to 1200°C, shows that both lignins release water, carbon dioxide, carbon monoxide, methane and methanol as temperatures rise, with both lignins showing pronounced maxima in the Gramm-Schmidt plots for methane or methanol around 400°C. However, a significant difference between the materials is observed with the detection of a strong carbonyl peak in the evolution products of the ML, with acetone not detected as a degradation product of organosolv lignin. This is considered to be associated with acetone evolution, arising from of scission of the hydroxypropyl substituent present in the ML structure. Other detail differences in the spectra of the degrading material have been related to the changes in the respective skeletal structures and again the differences in volatile degradation products confirm that there are important differences in the underlying reaction mechanisms.

The differences in the degradation processes are further reflected in the dielectric properties of the partially degraded materials where loss maxima occur at different temperatures, and show different degrees of frequency dependence. A significant observation here is the difference in conductivity, where the higher values observed with the OSL is thought to arise from cross-linking between adjacent benzene rings, whereas with the modified lignin lower conductivity is associated with intrinsically less conductive intermolecular linkages. This is consistent with the aforementioned spectroscopy results.

Taken overall it is considered that the results demonstrate that the thermal decomposition of the two lignins, although superficially similar, follow significantly different paths at the molecular level. In both cases, on heating, there is competition between thermodynamic and kinetic factors, as fluidity initially increases facilitating reaction, but spectroscopy and thermo-mechanical and thermo-electric analysis show that the reactions follow different paths and lead to structurally different products. With the more reactive OSL it appears to be the case that there is a greater tendency to form direct ring to ring crosslinks and this is very significant for the properties of the intended end product.

Acknowlegements

Mario Culebras, Anne Beaucamp, Baljinder K. Kandola, A. Richard Horrocks, Gianmarco Panzetti and Maurice N Collins acknowledge received funding from the BioBased Industries Joint Undertaking under the European Union's Horizon 2020 research and innovation programme under grant agreement No 720707. MC and MJS thank the Spanish Ministerio de Economía y Competitividad (MAT2015-63955-R) for partial financial help.

References

1. S. Laurichesse and L. Avérous, *Prog. Polym. Sci.*, 2014, **39**, 1266-1290.
2. P. Figueiredo, K. Lintinen, J. T. Hirvonen, M. A. Kostiainen and H. A. Santos, *Progress in Materials Science*, 2018, **93**, 233-269.
3. A. Barakat, F. Monlau, J.-P. Steyer and H. Carrere, *Bioresour. Technol.*, 2012, **104**, 90-99.
4. P. Pessala, E. Schultz, S. Luukkainen, S. Herve, J. Knuutinen and J. Paasivirta, *Pulp & paper mill effluent: environmental fate & effects*, 2004, 319-330.

5. M. M. Hossain, I. M. Scott, B. D. McGarvey, K. Conn, L. Ferrante, F. Berruti and C. Briens, *J. Anal. Appl. Pyrolysis*, 2013, **99**, 211-216.
6. C. Wang, S. S. Kelley and R. A. Venditti, *ChemSusChem*, 2016, **9**, 770-783.
7. H. Mainka, O. Täger, E. Körner, L. Hilfert, S. Busse, F. T. Edelmann and A. S. Herrmann, *Journal of Materials Research and Technology*, 2015, **4**, 283-296.
8. J. S. Lupoi, S. Singh, R. Parthasarathi, B. A. Simmons and R. J. Henry, *Renewable and Sustainable Energy Reviews*, 2015, **49**, 871-906.
9. H. Zhu, W. Luo, P. N. Ciesielski, Z. Fang, J. Y. Zhu, G. Henriksson, M. E. Himmel and L. Hu, *Chem. Rev.*, 2016, **116**, 9305-9374.
10. A. D. Venica, C.-L. Chen and J. S. Gratzl, *Holzforschung*, 2008, **62**, 627-636.
11. A. Effendi, H. Gerhauser and A. V. Bridgwater, *Renewable and Sustainable Energy Reviews*, 2008, **12**, 2092-2116.
12. A. De Chirico, M. Armanini, P. Chini, G. Cioccolo, F. Provasoli and G. Audisio, *Polym. Degrad. Stab.*, 2003, **79**, 139-145.
13. R. Zhang, X. Xiao, Q. Tai, H. Huang and Y. Hu, *Polymer Engineering & Science*, 2012, **52**, 2620-2626.
14. L. Costes, F. Laoutid, S. Brohez, C. Delvosalle and P. Dubois, *Eur. Polym. J.*, 2017.
15. X. Pan, J. F. Kadla, K. Ehara, N. Gilkes and J. N. Saddler, *J. Agric. Food. Chem.*, 2006, **54**, 5806-5813.
16. H. G. Chae and S. Kumar, *Science*, 2008, **319**, 908-909.
17. A. A. Ogale, M. Zhang and J. Jin, *Journal of Applied Polymer Science*, 2016, **133**.
18. H. Mainka, L. Hilfert, S. Busse, F. Edelmann, E. Haak and A. S. Herrmann, *Journal of Materials Research and Technology*, 2015, **4**, 377-391.
19. Q. Sun, R. Khunsupat, K. Akato, J. Tao, N. Labbé, N. C. Gallego, J. J. Bozell, T. G. Rials, G. A. Tuskan and T. J. Tschaplinski, *Green Chemistry*, 2016, **18**, 5015-5024.
20. E. Frank, L. M. Steudle, D. Ingildeev, J. M. Spörl and M. R. Buchmeiser, *Angew. Chem. Int. Ed.*, 2014, **53**, 5262-5298.
21. G. F. Zakis, *Functional analysis of lignins and their derivatives*, Atlanta, 1994.
22. A. Gartner, G. Gellerstedt and T. Tamminen, *Nord. Pulp Pap. Res. J.*, 1999, **14**, 163-170.
23. J. Mijovic and C. F. W. Yee, *Macromolecules*, 1994, **27**, 7287-7293.
24. L. Garden and R. A. Pethrick, *Int. J. Adhes. Adhes.*, 2017, **74**, 6-14.
25. J. Jakobsen, A. Skordos, S. James, R. G. Correia and M. Jensen, *Appl. Compos. Mater.*, 2015, **22**, 805-822.
26. R. A. Pethrick and D. Hayward, *Prog. Polym. Sci.*, 2002, **27**, 1983-2017.
27. A. Schönhals and F. Kremer, in *Broadband dielectric spectroscopy*, Springer, 2003, pp. 59-98.
28. Y.-F. Huang, P.-T. Chiueh, W.-H. Kuan and S.-L. Lo, *Energy*, 2016, **100**, 137-144.
29. D. Beneroso, T. Monti, E. T. Kostas and J. Robinson, *Chem. Eng. J.*, 2017, **316**, 481-498.
30. F. Motasemi, M. T. Afzal, A. A. Salema, J. Mouris and R. M. Hutcheon, *Fuel*, 2014, **124**, 151-157.
31. N. Guigo, A. Mija, L. Vincent and N. Sbirrazzuoli, *Phys. Chem. Chem. Phys.*, 2009, **11**, 1227-1236.
32. S. Perticaroli, B. Mostofian, G. Ehlers, J. C. Neuefeind, S. O. Diallo, C. B. Stanley, L. Daemen, T. Egami, J. Katsaras, X. Cheng and J. D. Nickels, *Phys. Chem. Chem. Phys.*, 2017, **19**, 25859-25869.

33. H. H. Sait and A. A. Salema, *Fuel*, 2015, **161**, 239-247.
34. A. A. Salema, F. N. Ani, J. Mouris and R. Hutcheon, *Fuel Process. Technol.*, 2017, **166**, 164-173.
35. S. Guidara, H. Feki and Y. Abid, *J. Alloys Compd.*, 2016, **672**, 86-92.
36. R. H. Boyd, *The Journal of Chemical Physics*, 1961, **35**, 1281-1283.
37. F. Bellucci, M. Valentino, T. Monetta, L. Nicodemo, J. Kenny, L. Nicolais and J. Mijovic, *J. Polym. Sci., Part B: Polym. Phys.*, 1994, **32**, 2519-2527.
38. F. Bellucci, M. Valentino, T. Monetta, L. Nicodemo, J. Kenny, L. Nicolais and J. Mijovic, *J. Polym. Sci., Part B: Polym. Phys.*, 1995, **33**, 433-443.
39. J. Mijovic, F. Bellucci and L. Nicolais, *J. Electrochem. Soc.*, 1995, **142**, 1176-1182.
40. G. Gallone, J. Levita, S. Mijovic, S. Andjelic and P. A. Rolla, *Polymer*, 1998, **39**, 2095-2102.
41. A. Šantić, W. Wrobel, M. Mutke, R. D. Banhatti and K. Funke, *Phys. Chem. Chem. Phys.*, 2009, **11**, 5930-5934.
42. T. Yamaguchi, E. Nakahara, K. Sueda and S. Koda, *The Journal of Physical Chemistry B*, 2013, **117**, 4121-4126.
43. J. R. Sangoro and F. Kremer, *Acc. Chem. Res.*, 2011, **45**, 525-532.
44. M. Watanabe, D. Kodama, T. Makino and M. Kanakubo, *Journal of Chemical & Engineering Data*, 2016, **61**, 4215-4221.
45. N. Ghaouar, *J. Mol. Liq.*, 2018, **250**, 278-282.